RSC Advances

PAPER

View Article Online
View Journal | View Issue

Cite this: *RSC Adv.*, 2018, **8**, 10246

Design, synthesis and characterization of a novel bluish-green long-lasting phosphorescence phosphor $BaLu_2Si_3O_{10}:Eu^{2+}$, Nd^{3+}

Jie Liu,[ab] Gen Li,[ab] Haijie Guo,[ab] Dongwei Liu,[ab] Peng Feng[ab] and Yuhua Wang *[ab]

Through drawing upon a solid-state reaction, a newly proposed long-lasting phosphor $BaLu_2Si_3O_{10}:Eu^{2+}$, Nd^{3+} is presented and prepared in this work. The thermoluminescence properties of the phosphor are substantially extended, and the long-lasting phosphorescence behavior is markedly intensified by virtue of the consolidation of Nd^{3+} ions which serve as trap centers. In line with density functional theory calculations, the conduction band is mostly composed of Lu 5d states while the Ba 5d states only have a tiny contribution. We analyzed the relationship between the phosphor's electronic structure and its optical properties. The photoluminescence emission spectrum shows a blue emitting band with a wide asymmetric property and an extremum of 426 nm, arising from the 5d–4f transitions of the Eu^{2+} ions which occupy the Ba and Lu sites. It is asserted that the long-lasting phosphorescence of the Eu^{2+} ions which take up both Ba and Lu sites stems from the special form of conduction band and the occupying environment of the emission center. Yet, they have different contributions and induce an interesting phenomenon in which the blue emitting phosphor shows a bluish-green phosphorescence. The long-lasting phosphorescence can last in excess of 6 h at the recognized intensity level (0.32 mcd m^{-2}) after excitation for 10 min. This work provides a new way of thinking for the development of multicolored LLP materials. This work analyzes and sheds light on the specific courses and provides a likely mechanism for the process.

Received 27th January 2018
Accepted 23rd February 2018

DOI: 10.1039/c8ra00842f

rsc.li/rsc-advances

1. Introduction

Long-lasting phosphorescence (LLP) is an optical phenomenon of great significance. Luminescence can be observed after ceasing the excitation after a couple of minutes and probably persists over a longer period of time of several hours.[1,2] Under excitation, energy can be stored and absorbed by LLP materials (inclusive of artificial light and sunlight). Subsequently, the stored and absorbed energy can be released as persistent visible light under thermal stimulation, commonly at room temperature.[3,4] LLP materials have aroused considerable attention and have been applied in extensive important fields by virtue of its prominent characteristics which include being recyclable, energy saving, and eco-friendly.[5] Initially, LLP materials were adopted for night-time displays, traffic signs, in or on buildings, in public places, for emergency signs, and security signs.[6] Additionally, the foregoing materials have been adopted in structural damage sensors, radiation detectors, and optical storage media.[7] Thus far, LLP materials have been adopted in a growing number of fields to address relevant challenges, such as in *in vivo* bio-imaging, medical diagnostics and solar energy utilization, *etc.*[8]

Moreover, large numbers of LLP materials have been developed and reported. LLP materials colored red, green and blue are primarily highlighted and discussed with a predominant amount of the research reported adopting these materials for a particular purpose. Theoretically, any color material can be attained through blending these three predominant colors and changing their proportions.[9–12] Yet, implementing the mentioned approach is difficult. Although two of the tricolor LLP materials, blue ($CaAl_2O_4:Eu^{2+}$, Nd^{3+}, >24 h) and green ($SrAl_2O_4:Eu^{2+}$, Dy^{3+}, >24 h), are very bright and can be adopted for use in the market, red LLP materials are overall inadequate when adopted for a particular purpose.[13,14] Making the various components consistent with each other during the phosphorescent decay can be hard and ensuring that the color of the phosphorescence is uniform can be difficult. Furthermore, a single source of excitation can be inefficient in exciting the majority of LLP materials.[15,16]

In this regard, newly proposed LLP materials consisting of multiple colors will be critically and urgently explored and developed. Currently, there is a growing interest in silicate-based luminescent materials due to their excellent chemical stability, thermal stability, weather resistance, and low

[a]*Department of Materials Science, School of Physical Science and Technology, Lanzhou University, Lanzhou, 730000, PR China. E-mail: wyh@lzu.edu.cn; Fax: +86 931 8913554; Tel: +86 931 8912772*

[b]*Key Laboratory for Special Function Materials and Structural Design of the Ministry of Education, Lanzhou University, Lanzhou 730000, China*

temperature synthesis.[17,18] In 2010, M. Wierzbicka-Wieczorek *et al.* initially developed and reported the trisilicates $BaRe_2Si_3O_{10}$ (Re = Sc, Yb, Er, and Gd).[19] The topological structure of the $BaRe_2Si_3O_{10}$ trisilicates consists of trisilicate Si_3O_{10} groups in the shape of a horseshoe and ReO_6 octahedra distorted by zigzag chains of edge-sharing. Subsequently, the foregoing trisilicate compounds, *e.g.* $BaSc_2Si_3O_{10}$ and $BaY_2Si_3O_{10}$ are adopted to synthesize numerous versatile lanthanon doped phosphors. Additionally, the application of these phosphors in white LEDs has been investigated, as well as their photoluminescent properties.[20–24] In 2014, the bivalent Eu^{2+} doped $BaM_2Si_3O_{10}$:Eu^{2+} (M = Sc, Lu) phosphor was prepared and proposed by Jakoah Brgoch *et al.*[25] In 2016, Kai Li *et al.* reported the preparation and photoluminescent properties of the tervalent Ce^{3+} and Tb^{3+} co-doped $BaLu_2Si_3O_{10}$ phosphor.[26] The $BaLu_2Si_3O_{10}$ phosphor has prominent luminescence properties, which has aroused massive research interest. Until now, as indicated by a literature review, no papers have studied the LLP properties of this phosphor. Traps are significant for photoenergy storage of persistent and thermo-stimulated phosphors. Suitable trap depths and trap densities are beneficial for improving LLP properties. Co-doping Re^{3+} ions counts as one of the most frequently adopted approaches to generate new traps or update the internal properties of traps arising from nonequivalent substitution. As Dorenbos' theory indicates that Nd^{3+} ions count as adequate traps, Nd^{3+} ions are deemed trap centers and can be incorporated into $BaLu_2Si_3O_{10}$:Eu^{2+} hosts.[27] Based on the above reasons, we have synthesized a LLP $BaLu_2Si_3O_{10}$:Eu^{2+}, Nd^{3+}phosphor. In this work, the electronic structure, photoluminescence, and phosphorescence properties of this phosphor are investigated systematically and shed light on.

2. Experimental

2.1 Synthesis

Following a frequently adopted method using high-temperatures in the solid state, this work fabricated the desired samples $Ba_{1-2x}Lu_2Si_3O_{10}$:xEu^{2+}, xNd^{3+} (x = 0, 0.004, 0.006, 0.008, 0.01 0.02 and 0.03, respectively presented as S1 to S6) whereby the raw materials were Eu_2O_3 (99.99%), Nd_2O_3 (99.99%), SiO_2 (99.99%), and $BaCO_3$ (99.99%). The relative raw materials were mixed in stoichiometric amounts and intensively ground uniformly in an agate mortar for 40 min, while incorporating an adequate amount of ethanol. The mixture was placed in alumina crucibles and sintered for 5 h at 1400 °C (N_2 : H_2 = 95 : 5) in a reducing atmosphere in a tube furnace powered by electricity. After calcining, the temperature of the samples was reduced within the furnace to room temperature and ground a second time for further application.

2.2 Characterization

These samples were characterized by powder X-ray diffraction (XRD) using a Rigaku diffractometer featuring Ni-filtered Cu Kα radiation at scanning steps of 0.02° with the 2θ value ranging from 10° to 80°. This enabled the overall phase structures of the samples to be examined. Through employing a F30 S-TWIN electron microscope (Tecnai™G2, FEI Company) high-resolution transmission electron microscopy (HRTEM) images, transmission electron microscopy (TEM) images, and an energy dispersive X-ray spectroscopy (EDX) spectrum were attained. Using a UV-Vis spectrophotometer (PE Lambda 950) and a sample of $BaSO_4$an ultraviolet-visible (UV-vis) diffuse reflectance spectra (DRS) was attained and used as a reference. A Xe-900 xenon arc lamp (450 W), with a FLS-920T fluorescence spectrophotometer as the source of excitation, was used to measure the luminescence decay curves, the LLP spectra, the photoluminescence excitation (PLE), and the photoluminescence emission (PL). 1 nm was established as the scanning step. 10 min after irradiating the samples with ultraviolet light a PR305 long afterglow instrument was used to measure the decay curve of the LLP. TL curves were provided using a FJ-427A TL meter (Beijing Nuclear Instrument Factory) with a heating rate of 1 K s^{-1} and a temperature range of 20 to 400 °C. In this work, UV light was used to irradiate 0.0020 g samples which had been pressed into pellets for 5 min prior to measuring. The photographs of $BaLu_2Si_3O_{10}$:Eu^{2+} and $BaLu_2Si_3O_{10}$:Eu^{2+}, Nd^{3+} under/after UV irradiation were taken in a dark room by a common digital camera with certain parameter settings (exposure time, ISO value, and aperture value). With the exception of the TL curves, these measurements were conducted at room temperature. Through using the CASTEP code and abiding by density functional theory, this work calculated the electronic structure adopted by $BaLu_2Si_3O_{10}$. Among the theories of density function, this work selected the local-density approximations (LDA).

3. Results and discussion

3.1 XRD patterns and Rietveld refinement

XRD was used to ascertain the phase purity adopted by the prepared samples. Given that the structure of $BaLu_2Si_3O_{10}$ has never previously been proposed in literature, this work references the crystallographic data and initial model structure with the purpose of refining them for $BaYb_2Si_3O_{10}$ (ICSD 17781). The representative XRD patterns for the relative samples are presented in Fig. 1a (S1–S6). All of the diffraction peaks are used as a standard reference for the $BaYb_2Si_3O_{10}$ (ICSD 17781) compound.[26] No impure phases were detected in the attained samples, which indicates that a single phase is taken up by all of the attained samples, and the Eu^{2+} and Nd^{3+} ions are successfully incorporated into the $BaLu_2Si_3O_{10}$ host. The XRD pattern of the $BaLu_2Si_3O_{10}$ host is presented in Fig. 1b on the basis of the Rietveld structural refinement which was attained using the Materials Studio program. The background, the experimental pattern and the calculated pattern are denoted by a yellow solid line, black crosses, and a red solid line, respectively. The Bragg reflection positions taken up by the acquired pattern are indicated by short vertical pink lines. At the bottom, the blue line shows how the calculated and experimental results are different from each other. Rietveld refinement effectively examines how atoms are positioned in a primitive cell. The residual factors are R_{wp} = 13.78%, R_p = 9.75% and χ^2 = 3.127, which demonstrate that the refined results are reliable. The refinement results

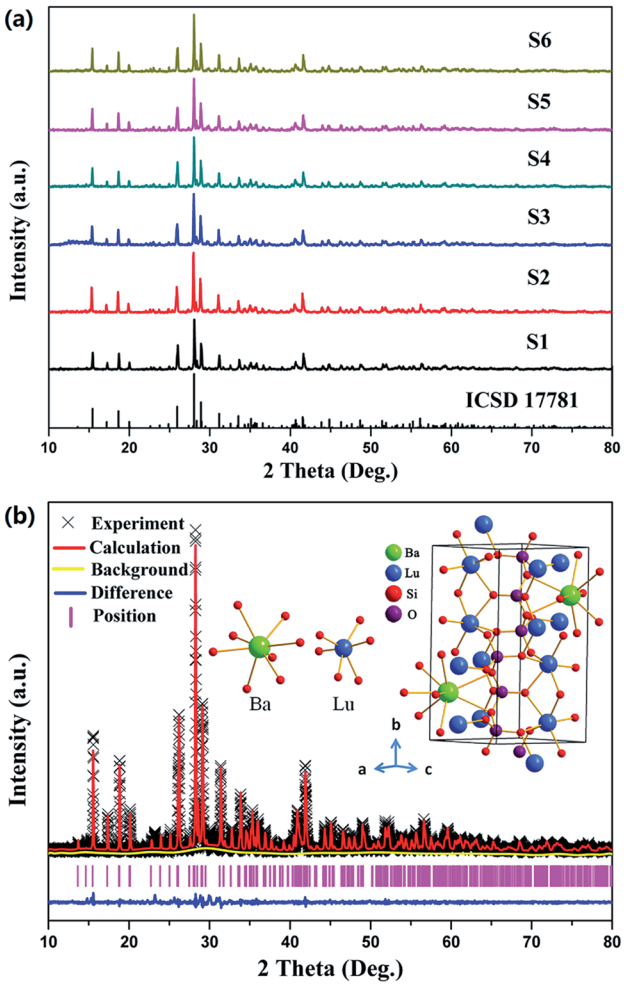

Fig. 1 (a) XRD patterns for $Ba_{1-2x}Lu_2Si_3O_{10}$:xEu^{2+}, xNd^{3+} ($x = 0$, 0.004, 0.006, 0.008, 0.01 0.02 and 0.03). (b) XRD refinement and the crystal structure of the $BaLu_2Si_3O_{10}$ host.

confirm that the compound is in the monoclinic space group $P2_1/m$ (no. 11) with cell parameters $a = 5.3541(1)$ Å, $b = 12.1224(3)$ Å, and $c = 6.7829(2)$ Å. The final refinement results indicate that this phosphor has two diverse cations, namely 8-coordinated Ba^{2+} ($r = 1.42$ Å) and 6-coordinated Lu^{3+} ($r = 0.861$ Å), presented in Fig. 1b. Distorted SiO_4 tetrahedra which form corner-sharing zig-zag trimers are contained in the crystal structure. Two Si^{4+} cations are given which are crystallographically independent. Through adopting two highly distorted edge-sharing LuO_6 octahedra, this work connects the foregoing SiO_4 trimers.[27] Generally, the radii difference between the two cations primarily determines whether the doped ions can substitute for the host cation.[25] The percentage difference in ionic radii between the substituted and the doped ions should be less than 30%.[28] The equation below can calculate the difference between the possible substituted ions (Ba^{2+}, Lu^{3+}) and the doped rare ions (Eu^{2+}, Nd^{3+}) in radius percentage.[29]

$$Dr = 100 \times [Rm(CN) - Rd(CN)]/Rm(CN) \quad (1)$$

Table 1 The radius and Dr values between Eu^{2+}/Nd^{3+} and Ba^{2+}/Lu^{3+}

	CN = 8 Ba^{2+}, $R = 1.420$ Å	CN = 6 Lu^{3+}, $R = 0.861$ Å
Eu^{2+}	$R = 1.250$ Å, Dr = 12%	$R = 1.170$ Å, Dr = 35%
Nd^{3+}	$R = 1.109$ Å, Dr = 22%	$R = 0.983$ Å, Dr = 14%

where Dr is the radius percentage difference; CN is the coordination number; Rm(CN) is the radius of the host cation; and Rd(CN) is the radius of the doped ion. The radii and calculated values of Dr between Eu^{2+}/Nd^{3+} and Ba^{2+}/Lu^{3+} are shown in Table 1. In light of calculated results from empirical equations, it can be deduced that Nd^{3+} ions could enter into both Ba and Lu sites while Eu^{2+} ions only seem to enter into the Ba sites.

3.2 Scanning electron microscopy and transmission electron microscopy analyses

The morphology of the two selected $BaLu_2Si_3O_{10}$ host and $BaLu_2Si_3O_{10}$:Eu^{2+}, Nd^{3+} samples was detected using SEM technology. As shown in Fig. 2a and c, the morphologies of these two samples are similar to each other. As shown, the blocky particles are irregularly shaped and approximately 2–10 μm in size, making their form and structure suitable for the fabrication of phosphors. The elemental composition of the $BaLu_2Si_3O_{10}$ host was investigated by EDX spectroscopy and the spectrum is shown in Fig. 2b. It confirms the presence of Ba, Lu, Si, and O in the $BaLu_2Si_3O_{10}$ sample. The elements of C and Cu come from the carbon membrane. The distance between the crystal planes reaches 0.325 nm, which is consistent with the (002) planes of

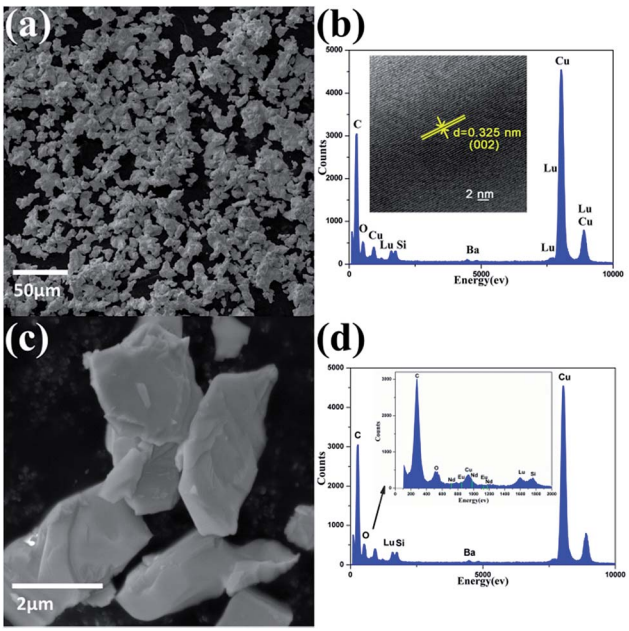

Fig. 2 (a) SEM images of the $BaLu_2Si_3O_{10}$ host. (b) EDX spectrum of the $BaLu_2Si_3O_{10}$ host. (Inset) HRTEM images of the $BaLu_2Si_3O_{10}$ host. (c) SEM images of $BaLu_2Si_3O_{10}$:Eu^{2+}, Nd^{3+}. (d) EDX spectrum of $BaLu_2Si_3O_{10}$:Eu^{2+}, Nd^{3+}. (Inset) Regional area with high resolution.

$BaLu_2Si_3O_{10}$ in Fig. 2b (inset).[30] In addition, the elemental composition of $BaLu_2Si_3O_{10}$:Eu^{2+}, Nd^{3+} was also investigated by EDX spectroscopy with the spectrum shown in Fig. 2d. As shown in Fig. 2d (inset), the elements of Eu and Nd are also detected.

3.3 Band structure

Fig. 3a–d show the computations of $BaLu_2Si_3O_{10}$ abiding by the density functional theory and on the basis of the crystal structure refinement. This paper selects the LDA as the theoretical basis of the density function. The relevant compound takes on an indirect bandgap which reaches approximately 4.843 eV, with the conduction band (CB) peaking at the G point and the valence band (VB) peaking at the D point of the Brillouin zone, which suggests that this is an appropriately wide bandgap for Eu^{2+} to serve as a center to emit light and for Nd^{3+} to serve as a trap center. The electronic structure taken on by the valence band primarily stems from O 2p states, whereas the conduction band is mostly encompassed by Lu 5d states. It is worth mentioning that Ba 5d states also have a tiny contribution to the conduction band. This special band structure characteristic has great effects on the phenomena of photoluminescence and phosphorescence.

3.4 UV-visible diffuse reflectance spectrum

Fig. 4 shows the DRS of the undoped $BaLu_2Si_3O_{10}$ host and concentration gradient samples of $BaLu_2Si_3O_{10}$:Eu^{2+}. For the host, the absorption in the ultraviolet region ranging from 200 to 400 nm arises from the valence-to-conduction band. For the samples of $BaLu_2Si_3O_{10}$:Eu^{2+}, the feature absorbance peaks of 290 nm and 325 nm are consistent with the excitation peaks as shown in Fig. 5a, which are attributed to the Eu^{2+} ions. The observed white color of the sample is a consequence of the spectral range being in the visible region. Kubelka–Munk-transformed DRS of the $BaLu_2Si_3O_{10}$ host, in line with the formula of $[F(R) \times h\nu]^n = A(h\nu - E_g)$, is presented in the inset of Fig. 4 where $F(R)$ is the Kubelka–Munk function with $F(R) = (1 - R)^2/2R$; R is the observed reflectance in the DRS; $n = 1/2$ for an indirect allowed transition, or 2 for a direct allowed transition, in this case n equals 1/2 according to the above calculated results of the band structure for $BaLu_2Si_3O_{10}$; A is the proportional constant; ν is the photon energy; and E_g is the value of the host bandgap.[29] By adopting the methods proposed by Cao *et al.*[31] the optical bandgap energy of $BaLu_2Si_3O_{10}$ is determined to be 5.5420 eV by extrapolation to $F(R) = 0$. It is expected that

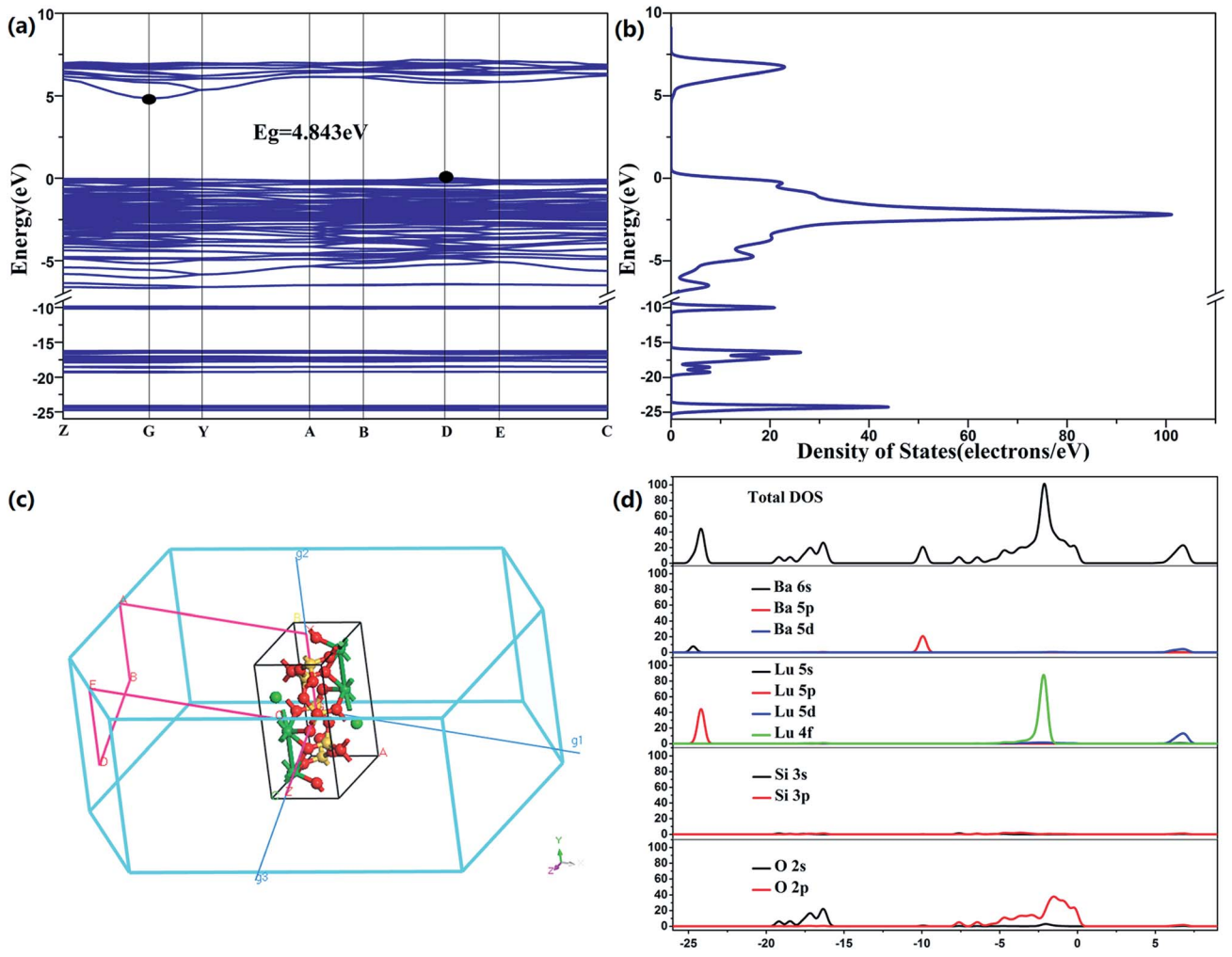

Fig. 3 (a) Band structure of $BaLu_2Si_3O_{10}$. (b) Density of states. (c) Brillouin zone. (d) Total and partial density of states.

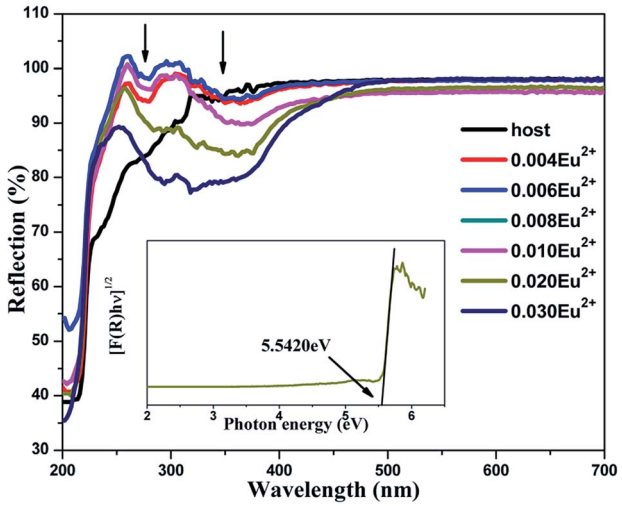

Fig. 4 DRS of the undoped $BaLu_2Si_3O_{10}$ host and concentration gradient samples of $BaLu_2Si_3O_{10}$:Eu^{2+}. (Inset) A curve of $[F(R) \times h\nu]^{1/2}$ *vs.* $h\nu$ for $BaLu_2Si_3O_{10}$.

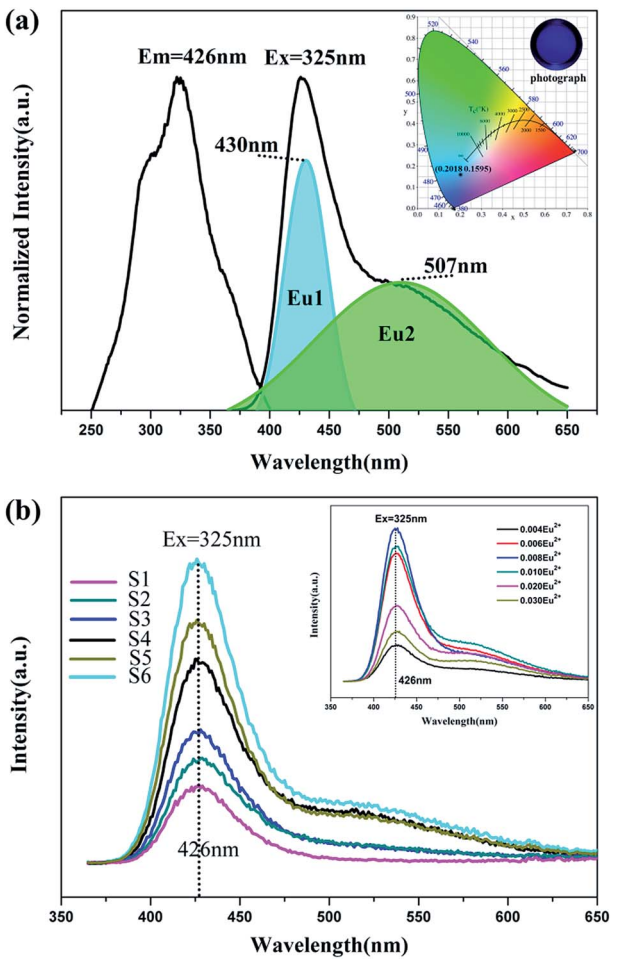

Fig. 5 (a) Excitation and emission spectra of $BaLu_2Si_3O_{10}$:$0.008Eu^{2+}$. (Inset) CIE chromaticity diagram and photographs of the $BaLu_2Si_3O_{10}$:$0.008Eu^{2+}$, $0.008Nd^{3+}$ phosphor excited at 325 nm. (b) Emission spectra of concentration gradient samples of $BaLu_2Si_3O_{10}$:Eu^{2+}, Nd^{3+}. (Inset) Emission spectra of concentration gradient samples of $BaLu_2Si_3O_{10}$:Eu^{2+}.

the value of the optical bandgap surpasses that of the previously calculated bandgap of approximately 4.843 eV as the local-density approximation depends less on the bandgap size and spin–orbit coupling of Lu^{3+} which has not been considered.[32]

3.5 Photoluminescence and phosphorescence properties

The emission and excitation spectra for the $BaLu_2Si_3O_{10}$:Eu^{2+} phosphor at room temperature is presented in Fig. 5a. The excitation spectrum that was monitored at 426 nm shows a broad excitation band ranging from 250 nm to 400 nm which arises from the $4f^7$–$4f^65d^1$ transition of Eu^{2+} ions. Two primary peaks at 290 nm and 325 nm which are contained in the broad band show that Eu^{2+} ions are present and that their role is as an emission center. In the case of a 325 nm optimal excitation, the material merely shows one wide asymmetric band with a long shoulder peaking at 426 nm. Such an emission peak arises from the Eu^{2+} ions undergoing equally allowed electronic $4f^65d^1$-$4f^7$ transitions, which is considerably affected by the lattice of the host.[30] In light of calculated results from the empirical equation, it can be deduced that Eu^{2+} ions only seem to access the Ba sites. However, on the basis of the analysis performed on the emission and excitation spectra, the incorporated Eu^{2+} ions could take up both Lu and Ba sites in the $BaLu_2Si_3O_{10}$ host. Accordingly, the emission centers fall into two types. In this regard, this work adopts Gaussian deconvolution which takes into account the emission spectrum of the $BaLu_2Si_3O_{10}$:Eu^{2+} phosphor being widely asymmetric, and the spectrum is compatible with two peaks at 507 nm and 430 nm. As the higher emission intensity shown by Eu1 in contrast to Eu2 elucidates, the Eu^{2+} ions preferably take up Ba sites instead of Lu sites. Fig. 5a presents (0.2018, 0.1595) as the CIE chromaticity coordinate for $BaLu_2Si_3O_{10}$:Eu^{2+} and blue as the color, which is acquired from the spectrum for emitting light whereby the calculation of the chromaticity coordinate follows the CIE1931 (Commission International de l'Eclairage France) system. As shown in Fig. 5b as the concentration of Nd^{3+} ions increases the emission spectra of $BaLu_2Si_3O_{10}$:Eu^{2+}, Nd^{3+} merely show one band being asymmetrically wide, which is similar to that of the single doped sample. As shown in Fig. 5b (inset), all doped samples have a broad asymmetric emission peak at 426 nm with a long shoulder. It also means Eu^{2+} ions fill both Ba and Lu sites. As the doping concentration increases the brightness increases and then decreases and shows $BaLu_2Si_3O_{10}$:$0.008Eu^{2+}$ to be the best doped sample. Additionally, this work fails to observe the representative emissions of the Nd^{3+} ions. As the foregoing results indicate, trivalent lanthanide ions Nd^{3+} are not deemed emission centers in $BaLu_2Si_3O_{10}$:Eu^{2+}, Nd^{3+} but are centers for trapping in numerous LLP phosphors.[30]

Fig. 6a shows the phosphorescence spectra of $BaLu_2Si_3O_{10}$:$0.008Eu^{2+}$, $0.008Nd^{3+}$ at different times after removing the excitation source. Interestingly, the profiles do not change with the phosphorescence decay time, but are greatly different from the emission profiles. This interesting phenomenon indicates that the LLP originates from both emissions (Eu_{Lu} and Eu_{Ba}) but they have very different contributions during the LLP process. In Fig. 6b, the phosphorescence spectrum of $BaLu_2Si_3O_{10}$:$0.008Eu^{2+}$,

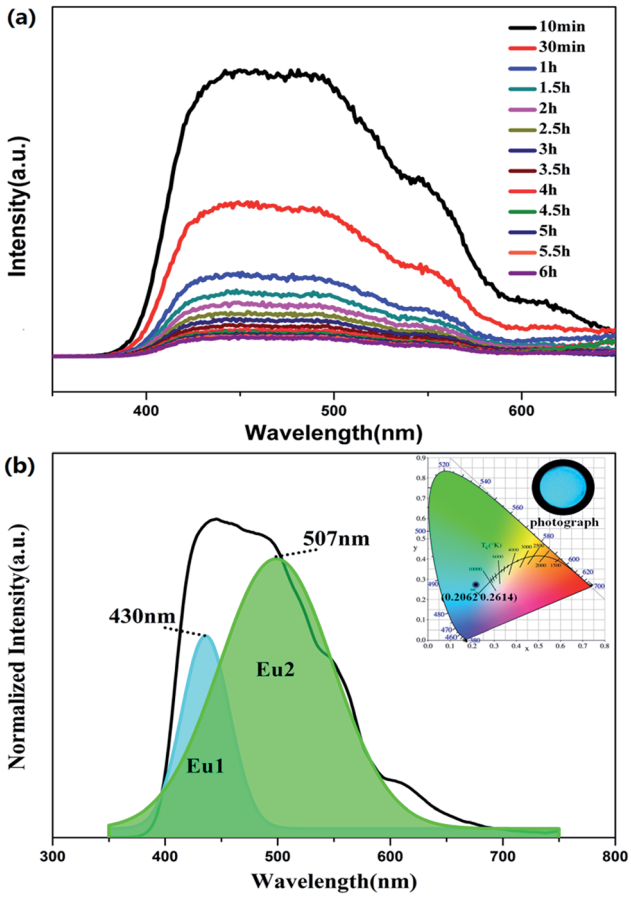

Fig. 6 (a) Phosphorescence spectrum of $BaLu_2Si_3O_{10}$:0.008Eu^{2+}, 0.008Nd^{3+}. (b) Phosphorescence spectra of $BaLu_2Si_3O_{10}$:0.008Eu^{2+}, 0.008Nd^{3+} 30 min after the removal of the excitation source. (Inset) CIE chromaticity diagram and photograph of the phosphorescence spectrum for the $BaLu_2Si_3O_{10}$:0.008Eu^{2+}, 0.008Nd^{3+} phosphor, excited at 325 nm.

0.008Nd^{3+} which was measured 30 min after the source of excitation was switched off is processed by Gaussian deconvolution and is consistent with two peaks at 430 nm and 507 nm, which is similar to the PL spectrum. The phosphorescence CIE chromaticity coordinate is (0.2062, 0.2614) and the color is bluish-green, as shown in the inset of Fig. 6b. The PL color is blue but the phosphorescence color is bluish-green, indicating that the phosphorescence is derived from the 5d–4f transition of Eu^{2+} ions in the Ba and Lu sites. Eu_{Lu} has a greater contribution during the LLP process, so the color of phosphorescence tends to be green, rather than blue.

3.6 Luminescence decay curves

To demonstrate that the phosphorescence stems from the Eu_{Lu} emission in the current $BaLu_2Si_3O_{10}$ host, luminescence decay curves were measured at an excitation of 325 nm and monitored at 426 and 507 nm. The results are shown in Fig. 7. The luminescence decay curves were able to be adjusted by a double-exponential mode and the average luminescence decay time τ could be ascertained from the formula below.[33]

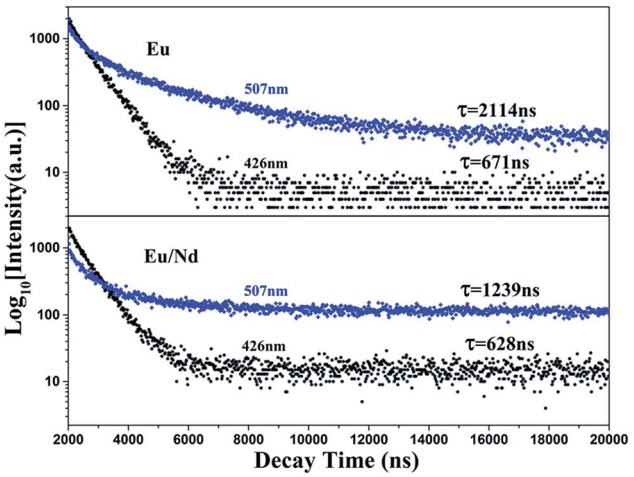

Fig. 7 Luminescence decay curves of $BaLu_2Si_3O_{10}$:Eu^{2+} and $BaLu_2Si_3O_{10}$:Eu^{2+}, Nd^{3+} excited at 325 nm and monitored at 426 nm and 507 nm.

$$\tau = (A_1\tau_1^2 + A_2\tau_2^2)/(A_1\tau_1 + A_2\tau_2) \quad (2)$$

where A_1 and A_2 are constant and τ_1 and τ_2 are the two exponential components of the fitting luminescence decay curve. Table 2 lists the fitting parameters specifically. In line with the equation above and the fitting parameters, the average luminescence decay times monitored at 426 and 507 nm were calculated to be 671 and 2114 ns for the $BaLu_2Si_3O_{10}$:Eu^{2+} phosphor, and 638 and 1239 ns for the $BaLu_2Si_3O_{10}$:Eu^{2+}, Nd^{3+} phosphor, respectively. We found that both the luminescence decay times monitored at 426 and 507 nm are characteristic of the 5d–4f allowed transition of Eu^{2+}, indicating that the green phosphorescence at 507 nm indeed originates from the Eu^{2+} emission, rather than from some defect levels.[34] The Eu^{2+} luminescence decay time decreases with the introduction of Nd^{3+} ions. The reason is that with the introduction of Nd^{3+} ions there is an inequivalence of substitution which leads to lattice distortion and causes lots of defects. Those defects could play a role as energy traps, where the energy from Eu^{2+} ions can transfer. This new approach for energy transfer causes a decrease in the luminescence decay time. Furthermore, the dual-exponential curve fitting arising from the spectral overlap of the two emission bands and can support the statement that Eu^{2+} occupies both the Ba and Lu sites in $BaLu_2Si_3O_{10}$.[30]

Table 2 The fitting parameters of the luminescence decay curves of $BaLu_2Si_3O_{10}$:Eu^{2+} and $BaLu_2Si_3O_{10}$:Eu^{2+}, Nd^{3+} excited at 325 nm and monitored at 426 nm and 507 nm.

Sample	λ_{em} (nm)	τ_1 (ns)	τ_2 (ns)	A_1	A_2
Eu^{2+}	426	722.81	235.58	1438.98	524.39
	507	2618.30	470.54	545.66	930.57
Eu^{2+}, Nd^{3+}	426	671.06	160.98	1584.67	448.23
	507	1606.05	288.46	313.56	673.59

3.7 LLP decay curves

As presented in Fig. 8a, this work measured the LLP decay curves for all of the as-synthesized samples (S1–S6) in order to delve into the decay performance of the $BaLu_2Si_3O_{10}:Eu^{2+}$, Nd^{3+} emission. The decay process of the LLP is encompassed by a slow decay process and a fast decay process. Those fast decay processes occur initially and dominate the intensity at the very beginning, and the slow decay processes occur later which lead to the long term behavior.[35–38] This work, through adopting curve-fitting technology, analyzes the decay curves of the samples (S1–S6), and these curves are found to adequately match the following double-exponential equation.

$$I = A_1 \exp(-t/\tau_1) + A_2 \exp(-t/\tau_2) + A_0 \quad (3)$$

where I is the phosphorescence intensity, A_0, A_1 and A_2 are constants, t is time, and τ_1 and τ_2 are the decay times of the exponential components. Since the performance of LLP is chiefly determined by τ_2,[39] the τ_2 values for all of the samples are listed in Table 3. The value of τ_2 increases in the beginning and then decreases later with the increase in Eu^{2+} and Nd^{3+} ion content. They reach a maximum when the amount of the Eu^{2+} and Nd^{3+} ions reaches 0.008 mol. LLP decay curves of $BaLu_2Si_3O_{10}:Eu^{2+}$ are shown in the inset of Fig. 8a. The values peak when there is 0.008 mol of Eu^{2+} ions. The initial LLP intensity of $BaLu_2Si_3O_{10}$:0.008Eu^{2+}, 0.008Nd^{3+} is in the vicinity of 0.013 cd m^{-2} and its LLP can continue in excess of 6 h over an intensity level which is able to be recognized (0.32 mcd m^{-2}). The phosphorescence of $BaLu_2Si_3O_{10}$:0.008Eu^{2+} is only visible for 199 s by the naked eye, which indicates that the introduction of Nd^{3+} ions greatly optimizes the phosphorescence of $BaLu_2Si_3O_{10}$:0.008Eu^{2+}. The LLP decay curve of $BaLu_2Si_3O_{10}$:0.008Eu^{2+}, 0.008Nd^{3+} is also plotted as a function of reciprocal persistent luminescence intensity (I^{-1}) *versus* time (t), as presented in Fig. 8b. The detailed reasons are discussed later in the section on TL curves.

Table 3 Decay times for two exponential components of $Ba_{1-2x}Lu_2Si_3O_{10}:xEu^{2+}$, xNd^{3+} (x = 0, 0.004, 0.006, 0.008, 0.01 0.02 and 0.03)

Sample	A_0	A_1	τ_1 (s)	A_2	τ_2 (s)
S1	7.2266×10^{-4}	0.0110	55.5423	0.0054	1224.0458
S2	6.7820×10^{-4}	0.0086	62.6299	0.0046	1242.8820
S3	8.3097×10^{-4}	0.0170	60.0109	0.0065	1326.3692
S4	6.6350×10^{-4}	0.0093	50.3919	0.0037	1323.1464
S5	8.0447×10^{-4}	0.0150	55.4197	0.0061	1191.9548
S6	3.9931×10^{-4}	0.0022	26.1850	0.0012	236.5758

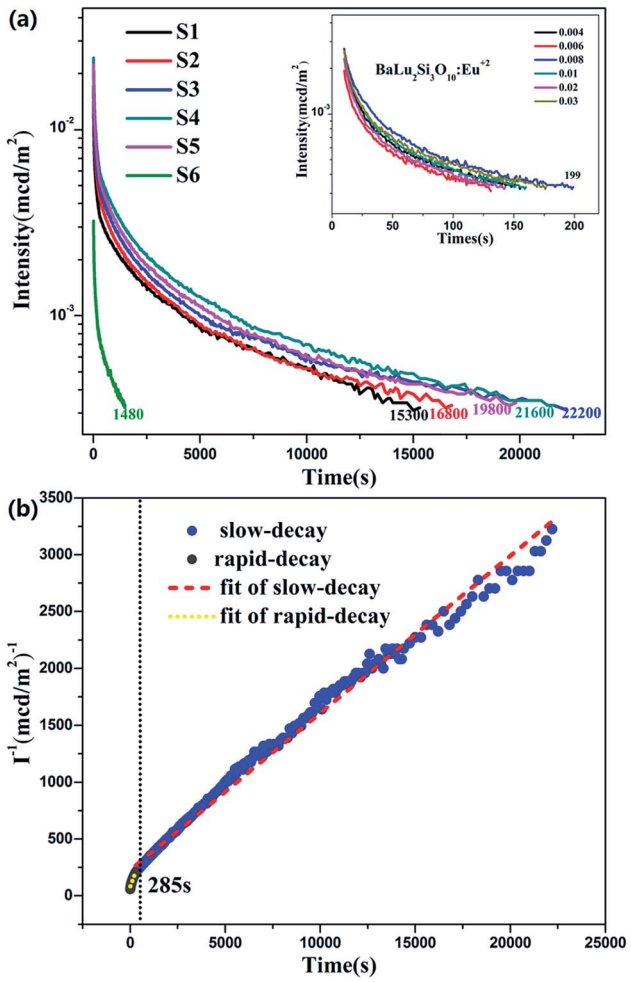

Fig. 8 (a) LLP decay curves of $BaLu_2Si_3O_{10}:Eu^{2+}$, Nd^{3+}. Inset: LLP decay curves of $BaLu_2Si_3O_{10}:Eu^{2+}$ (b) function of reciprocal LLP intensity (I^{-1}) *versus* time (t) of $BaLu_2Si_3O_{10}$:0.008Eu^{2+}, 0.008Nd^{3+} excited for 10 min.

3.8 Thermoluminescence curves

Trapping centers play a momentous role in the photo-energy storage of persistent and thermo-stimulated phosphors.[40] After removal of the excitation source, the captured charge carriers are able to escape due to thermal disturbance and are transferred to centers for luminescence, which triggers the phosphorescence. Accordingly, shallow depth traps are negatively and adversely affected by stabilizing the charge carriers, which considerably shortens the duration period of persistent luminescence. In contrast, the charge carriers that are captured by deep depth traps are extremely hard to release at room temperature, which leads to the defective performance of the LLP.[40–42] For this reason, as the appropriate trap depth is formed, a solid foundation is laid for attaining a perfect LLP performance. Meanwhile, the trap density is also a significant factor for LLP. To characterize the traps in our samples TL measurements were conducted on $BaLu_2Si_3O_{10}$:0.008 Eu^{2+} and $BaLu_2Si_3O_{10}$:0.008 Eu^{2+}, 0.008 Nd^{3+}, their TL curves are shown in Fig. 9, we only observe three very weak peaks in $BaLu_2Si_3O_{10}:Eu^{2+}$ and it is possible that the TL bands arise from intrinsic defects in the host as the Eu^{2+} ions are equally replaced by Ba^{2+} ions in $BaLu_2Si_3O_{10}$. Additionally, as the weak TL signal indicates, the concentration of carriers that is captured by the intrinsic defects is extremely low. When Nd^{3+} ions are co-doped, the intensity of the peaks are evidently enhanced, and the primary peak position moves to 330 K, meaning that the doping of the Nd^{3+} ions considerably elevates the defect levels. To further evaluate the trap states, the trap depths (E_t) and the trap densities (n_0) can be acquired from eqn (4) and (5).[43]

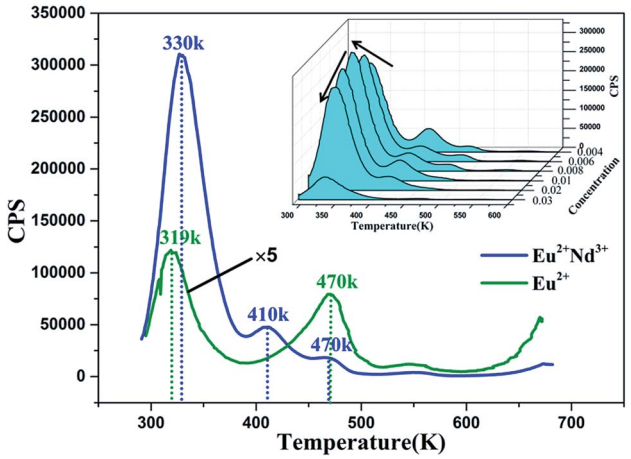

Fig. 9 TL curves of $BaLu_2Si_3O_{10}$:0.008Eu^{2+}, 0.008Nd^{3+} excited for 25 min. Inset: concentration gradient TL curves of $BaLu_2Si_3O_{10}$:Eu^{2+}, Nd^{3+} excited for 5 min.

$$E_t = [2.52 + 10.2 \times (\mu_g - 0.42)] \times (K_B T_m^2/\omega) - 2K_B T_m \quad (4)$$

$$n_0 = \omega I_m/\{\beta \times [2.52 + 10.2 \times (\mu_g - 0.42)]\} \quad (5)$$

Where I_m is the intensity of the TL peak, δ is the high-temperature half-width, τ is the low-temperature half-width, the asymmetry parameter $\mu_g = \delta/(\tau + \delta)$, β is the heating rate, K_B is the Boltzmann constant (1.38×10^{-23} J K^{-1}), T_m is the temperature of the TL peak, and ω is known as the shape parameter and is defined as $\omega = \tau + \delta$. As shown in Table 4, for the $BaLu_2Si_3O_{10}$:0.008Eu^{2+} sample, although the trap depth is appropriate for releasing the trapped carriers, the low trap density directly results in a brief LLP of 199 s. For $BaLu_2Si_3O_{10}$:0.008Eu^{2+}, 0.008Nd^{3+}, by co-doping with Nd^{3+} ions, more traps are generated with a suitable energy depth which greatly improves the duration of the LLP and the LLP brightness in the very beginning. This result suggests that co-doping indeed has a great effect upon the LLP performance of the phosphor.

3.9 LLP mechanism

Under normal conditions, for the majority of LLP materials, the color of the phosphorescence is identical to the color of the PL arising from the identical emission centers. Yet the blue emitting phosphors show a phosphorescence which is characterized as bluish-green in this paper. In line with the previous analysis, Eu^{2+} ions which occupy Ba and Lu sites serve as emission centers and Nd^{3+} ions which take up Ba sites serve as trapping centers in the co-doped samples. As these experiments overall indicate, this material provides highly-efficient trapping conditions. A probable LLP mechanism for forming the efficient bluish-green LLP in Eu^{2+} and Nd^{3+} co-doped $BaLu_2Si_3O_{10}$ is shown in Fig. 10. Under UV excitation, the $4f^7$ ground-state electrons of the Eu^{2+} ions are promoted to the $4f^65d^1$ excited state (excitation process 1). Partial electrons which are promptly excited are reincorporated with the Eu^{2+} ions excited on the Ba and Lu sites to produce luminescence (PL process 2). As most Eu^{2+} ions occupy the Ba sites and tiny Eu^{2+} ions occupy the Lu sites, the phosphor emits blue light. Simultaneously other excited electrons are able to move *via* the conduction band and are captured later by the traps (electron trapping process 3). When the electrons captured by shallow traps are thermally released at room temperature, they move back to the conduction band directly and a few of the captured electrons in deep traps escape through a quantum tunneling process. In view of the conduction band primarily being formed by Lu 5d states rather than Ba states, the released electrons prefer to transfer to the excited Eu^{2+} ions on the Lu sites which are in the same form of resonance and recombine with them, which gives rise to the green phosphorescence (LLP process 4). In short, it is the special form of the conduction band and the occupation situation of the emission centers that result in the interesting optical phenomenon.

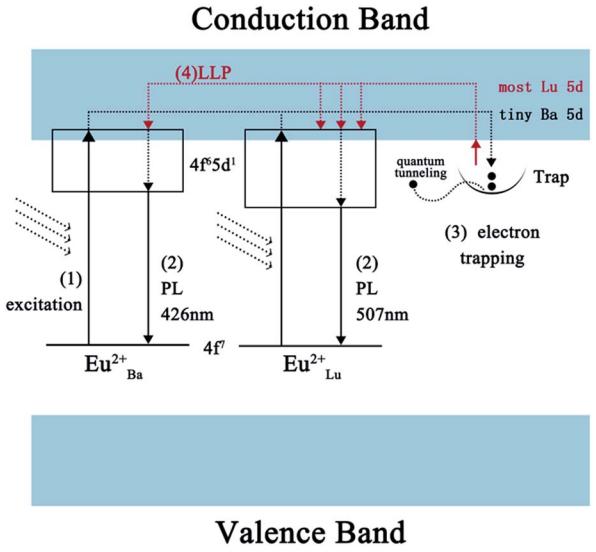

Fig. 10 A possible schematic diagram of the afterglow mechanism.

Table 4 TL parameters of $BaLu_2Si_3O_{10}$:0.008Eu^{2+} and $BaLu_2Si_3O_{10}$:0.008Eu^{2+}, 0.008Nd^{3+}

	Glow-peak parameters					TL parameters	
Sample	T_m (K)	T	δ	ω	μ_g	E_t (eV)	n_0
Eu^{2+}	319	19	23	42	0.55	0.75	2.65×10^5
Eu^{2+}, Nd^{3+}	330	21	27	48	0.56	0.71	3.75×10^6

4. Conclusions

In a nutshell, a newly proposed bluish-green emitting long-lasting phosphor with prominent LLP properties is successfully achieved *via* a high temperature solid state method. Eu^{2+} ions show a broad asymmetric emission band with a peak at 426 nm as it occupies both the Ba and Lu sites in $BaLu_2Si_3O_{10}$. The blue emitting phosphors show a kind of green phosphorescence phenomenon, which is induced mostly by the emission of Eu^{2+} ions occupying the Lu sites. Co-doping with Nd^{3+}

ions can effectively improve the LLP performance. The LLP can last more than 6 h above the recognizable intensity level (0.32 mcd m^{-2}). This work also provides direct experimental evidence that the conduction band is of critical significance for the course of LLP. And the analysis regarding this experimental work backs up the LLP mechanism. This new LLP material exhibits a 6 h LLP and has considerable potential for extensive applications.

Conflicts of interest

There are no conflicts to declare.

Acknowledgements

This work is supported by the National Natural Science Funds of China (Grant No. 51672115 and Grant No. 51372105). Thanks for the support of Chengguan district Lanzhou city science and technology development projects (project number: 2017-2-2).

Notes and references

1 Z. Pan, Y. Y. Lu and F. Liu, *Nat. Mater.*, 2012, **11**, 58–63.
2 C. N. Xu, T. Watanabe, M. Akiyama and X. G. Zheng, *Appl. Phys. Lett.*, 1999, **74**, 2414–2416.
3 D. Q. Chen, Y. Chen, H. W. Lu and Z. G. Ji, *Inorg. Chem.*, 2014, **53**, 8638–8645.
4 D. Q. Chen, *J. Eur. Ceram. Soc.*, 2014, **34**, 4069–4075.
5 T. Maldiney, C. Richard, D. Scherman and D. Gourier, *Chem. Mater.*, 2014, **26**, 1365–1373.
6 J. Wang, Q. Su and S. B. Wang, *J. Phys. Chem. Solids*, 2005, **66**, 1171–1176.
7 S. Lian, Y. Qi, C. Rong, L. Yu, A. Zhu, D. Yin and S. Liu, *J. Phys. Chem. C*, 2010, **114**, 7196–7204.
8 B. Wang, H. Lin, Y. L. Yu, D. Q. Chen, R. Zhang, J. Xu and Y. S. Wang, *J. Am. Ceram. Soc.*, 2014, **97**, 2539–2545.
9 T. Matsuzawa, Y. Aoki, N. Takeuchi and Y. Murayama, *J. Electrochem. Soc.*, 1996, **143**, 2670–2673.
10 H. J. Guo, W. B. Chen, W. Zeng and Y. H. Wang, *J. Mater. Chem. C*, 2015, **22**, 5844–5850.
11 Z. Hong, P. Zhang, X. Fan and M. Wang, *J. Lumin.*, 2007, **124**, 127–132.
12 V. K. Van den Eeckhout, P. F. Smet and D. Poelman, *J. Lumin.*, 2009, **129**, 1140–1143.
13 T. Matsuzawa, Y. Aoki, N. Takeuchi and Y. Murayama, *J. Electrochem. Soc.*, 1996, **143**, 2670–2673.
14 H. Yamamoto and T. Matsuzawa, *J. Lumin.*, 1997, **72–74**, 287–289.
15 I. P. Sahu, D. P. Bisen, N. Brahme, L. Wanjari and R. K. Tamrakar, *Res. Chem. Intermed.*, 2015, **41**, 8797–8814.
16 P. J. Wang, X. H. Xu, D. C. Zhou, X. Yu and J. B. Qiu, *Inorg. Chem.*, 2015, **54**, 1690–1697.
17 T. L. Barry, *J. Electrochem. Soc.*, 1968, **115**, 1181–1183.
18 Y. Lin, Z. Zhang, Z. Tang, X. Wang and Z. Zheng, *J. Eur. Ceram. Soc.*, 2001, **21**, 683–685.
19 M. Wierzbicka-Wieczorek, U. Kolitsch and E. Tillmanns, *Eur. J. Mineral.*, 2010, **22**, 245.
20 Q. Wang, G. Zhu, S. Y. Xin, X. Ding, J. Xu, Y. S. Wang and Y. H. Wang, *Phys. Chem. Chem. Phys.*, 2015, **17**, 27292–27299.
21 J. Q. Wang, W. R. Zhao, J. M. Zhong and L. C. Lan, *J. Mater. Sci.: Mater. Electron.*, 2014, **25**, 2162–2168.
22 J. Zhou and Z. G. Xia, *J. Mater. Chem. C*, 2015, **3**, 7552–7560.
23 W. R. Liu, C. C. Lin, Y. C. Chiu, Y. T. Yeh, S. M. Jang, R. S. Liu and B. M. Cheng, *Opt. Express*, 2009, **17**, 18103–18109.
24 J. Zhou and Z. G. Xia, *Opt. Mater.*, 2016, **52**, 116–122.
25 J. Brgoch, K. Hasz, K. A. Denault, C. K. H. Borg, A. A. Mikhailovsky and R. Seshadri, *Faraday Discuss.*, 2014, **176**, 333–347.
26 K. Li, S. S. Liang, H. Z. Lian, M. M. Shang, B. G. Xing and J. Lin, *J. Mater. Chem. C*, 2016, **4**, 3443–3453.
27 P. Dorenbos, *J. Phys.: Condens. Matter*, 2003, **15**, 8417.
28 M. Y. Peng, Z. W. Pei, G. Y. Hong and Q. Su, *J. Mater. Chem.*, 2003, **13**, 1202–1205.
29 R. D. Shannon, *Acta Crystallogr.*, 1976, **32**, 751–767.
30 G. Li, Y. H. Wang, H. J. Guo, J. Liu, D. W. Liu and P. Feng, *J. Lumin.*, 2017, **192**, 98–104.
31 G. Cao, L. K. Rabenberg, C. M. Nunn and T. E. Mallouk, *Chem. Mater.*, 1991, **3**, 149–156.
32 Y. Q. Li, Y. H. Wang, X. H. Xu, G. Yu and F. Zhang, *J. Electrochem. Soc.*, 2010, **157**, 39–43.
33 N. Ruelle, M. P. Thi and C. Fouassier, *Jpn. J. Appl. Phys.*, 1992, **31**, 2786–2790.
34 C. Y. Liu, Z. G. Xia, Z. P. Lian, J. Zhou and Q. F. Yan, *J. Mater. Chem. C*, 2013, **1**, 7139–7147.
35 J. Zhang, X. Ma, Q. Qin, L. Shi, J. Sun, M. Zhou, B. Liu and Y. Wang, *Mater. Chem. Phys.*, 2012, **136**, 320–324.
36 J. Wang, S. Wang and Q. Su, *J. Mater. Chem.*, 2004, **14**, 2569–2574.
37 R. Pang, C. Li, L. Shi and Q. Su, *J. Phys. Chem. Solids*, 2009, **70**, 303–306.
38 B. Lei, H. Zhang, W. Mai, S. Yue, Y. Liu and S. Man, *Solid State Sci.*, 2011, **13**, 525–528.
39 T. Wang, Y. H. Hu, L. Chen, X. J. Wang and G. F. Ju, *Radiat. Meas.*, 2015, **73**, 7–13.
40 J. Glodo and A. Wojtowicz, *J. Alloys Compd.*, 2000, **300**, 289–294.
41 T. Aitasalo, P. Deren, J. Hölsä, H. Junger, J. C. Krupa, M. Lastusaari, J. Legendziewicz, J. Niittykoski and W. Strek, *J. Solid State Chem.*, 2003, **171**, 114–122.
42 T. Kinoshita, M. Yamazaki, H. Kawazoe and H. Hosono, *J. Appl. Phys.*, 1999, **86**, 3729–3733.
43 R. Chen, *J. Appl. Phys.*, 1969, **40**, 570–585.

